Metrologia

A two-capillary viscometer for temperatures up to 473 K and pressures up to 100 MPa—operation and verification at low pressure

OPEN ACCESS
IOP Publishing | Bureau International des Poids et Mesures Metrologia
Metrologia **61** (2024) 035008 (15pp) https://doi.org/10.1088/1681-7575/ad435d

A two-capillary viscometer for temperatures up to 473 K and pressures up to 100 MPa—operation and verification at low pressure

Bahareh Khosravi[1,*], Anders Austegard[2], Sigurd W Løvseth[2], H G Jacob Stang[2] and Jana P Jakobsen[1]

[1] Norwegian University of Science and Technology, Trondheim, Norway
[2] SINTEF Energy Research, Trondheim, Norway

E-mail: bahareh.khosravi@ntnu.no

Received 3 June 2023, revised 23 April 2024
Accepted for publication 25 April 2024
Published 20 May 2024

Abstract

In this paper, we described the design and construction of a new two-capillary viscometer with several novel technical solutions for viscosity and density measurements. Our design, which is based on the low-pressure principle, featured numerous improvements in hardware and procedure that allowed the greatly extended range of pressure. The new design adopted a (2×2) capillary configuration, utilizing different combinations of four capillaries to enable viscosity measurements with a wide range of flow rates, temperatures, and pressures. The design temperature range is 213 K–473 K, and the pressure range is up to 100 MPa. The viscometer was specifically designed for measuring the viscosity of pure CO_2 and CO_2-rich mixtures, addressing the scarcity of data in conditions relevant to carbon capture, transport, and storage. Our facility is capable of viscosity measurements in different thermodynamic states; gaseous, liquid, supercritical, and critical regions. A commercial densimeter is integrated to measure density under the same temperatures and pressures. We aimed for a total uncertainty target of better than 0.03%. The performance of the viscometer was validated by measurements with pure CO_2 at 298.15 K and zero density. We observed a deviation of less than 0.03% between the reference viscosity of CO_2 of this work and accurately calculated data using *ab initio* quantum mechanics with a standard uncertainty of 0.2%. Our primary focus in this paper was to provide a detailed description of the design and construction of the apparatus, emphasizing improvements and introducing new solutions to other research groups in constructing similar instruments suitable for low- and high-pressure viscosity measurements with high accuracy.

Keywords: two-capillary viscometer, viscosity, CO_2

* Author to whom any correspondence should be addressed.

1. Introduction

In CO_2 capture, transport, and storage (CCS), comprehensive knowledge about the thermophysical properties is essential for the design, operation, and optimization of all the processes along the whole chain. Mathematical models are generally used to predict the necessary thermophysical properties. These properties are influenced by different variables, such as the stream composition and operational conditions. Since the CCS processes cover an expansive range of fluid conditions and involve multi-component mixtures, a single mathematical model cannot fulfill the requirement for providing highly accurate property estimates. The main reason being that the established models are limited by the extent of available experimental data and their high uncertainty. Limited experimental data contributes to significant uncertainties in model predictions. This uncertainty may result in additional safety margin in design, adding avoidable capital and operational costs for large-scale CCS [1]. Viscosity and density are two crucial thermophysical properties significant for CO_2 transport and storage processes. Viscosity is a crucial parameter for flow calculation, where the pressure drop is proportional to the viscosity. It is also needed for the Reynolds number to characterize the flow regime. Reservoir injectivity index, plume evolution, and storage efficiency also depend on the viscosity. In CO_2 enhanced oil recovery, the mobility of CO_2 into the reservoir depends strongly on the viscosity contrast. Viscosity has an impact on history-matching and seismic interpretation, long-term CO_2 migration, and potential for reservoir leakage. Several studies show that impurities can significantly affect the viscosity of CO_2, particularly close to the critical point, where a thermodynamic state transition occurs [2, 3]. Density is also required to estimate reservoir capacity, injection pressure, plume evolution and buoyancy migration in gravity-dominated systems [4]. Therefore, an accurate viscosity and density database for different types of impurities, and at a wide range of operating conditions is essential for developing more accurate models.

The long-term aim of the presented research work is to enable reduction of large-scale CCS project costs and associated risks by providing high-quality thermophysical property data at conditions relevant for CO_2 transport and storage. For this purpose, a new two-capillary viscometer has been designed and constructed to provide high accuracy measurements, covering the region of interest for CCS; temperature ranges between 213.15 K and 473.15 K, design pressures up to 100 MPa, Pure and mixed liquid, supercritical and gaseous states can be measured by the new apparatus. In addition, a commercial vibrating tube densimeter is combined with the viscometer for measurements of density at the same conditions as the viscosity measurements. The new apparatus will facilitate both closures of data gaps in density and enable direct conversion between kinematic and dynamic viscosity.

1.1. State of the art

Capillary viscometer as the most common instrument for viscosity measurements was introduced in 1840 by Poiseuille [5], who studied the flow of distillated water. Absolute viscosity of water at 293.15 K and atmospheric pressure which is still used as one of the two sources to establish the ISO was measured using a single capillary by Swindells *et al* in 1952 [6], reporting a viscosity value of 0.001 0019 (3) Pa·s. In 1985, Hoogland *et al* [7] developed a capillary-flow viscometer for the precise determination of the viscosity of gases near critical points. They modified the Poiseuille formula for compressible fluids, and measurements on sulfur hexafluoride were performed up to 10 kPa with standard uncertainty of about 0.1%. Besides, viscosity of nitrogen at several pressures and temperatures were measured for the purpose of calibrations. A broad survey of the various methods for viscosity measurements, in particular for different type of capillary viscometers, was presented by Kestin *et al* in 1973 and revised by Wakeham in 1991 [8, 9].

In 1993, a capillary viscometer was used to measure the viscosities of pure gaseous CO_2 and Ar-CO_2 mixtures. The accuracy achieved was within $\pm 0.7\%$ over the temperature range of 213 K–353 K, utilizing a ratio measurement method compared to pure Ar [10].

In 2004 [11], Berg described a quartz capillary flow meter (QCFM) for measuring gas flow rates below 1000 μmol s^{-1} with an uncertainty of less than 0.03%. The same work also introduced a hydrodynamic model based on the Hagen–Poiseuille equation with relevant correction factors for QCFM. In 2005 [12], Berg used the QCFM alternatively as a single capillary to measure the absolute viscosity of several gases at 298.15 K and atmospheric pressure. The estimated uncertainty was less than 0.04% at 298.15 K, where an independent flow rate measurement was required for the viscosity measurements. Ultimately, the uncertainty of the measurements was verified by comparing the measured viscosity data of helium using the QCFM with the predictions from the *ab initio* model [13]. The results showed that a new flow meter/viscometer could be constructed and calibrated using *ab initio* values for the viscosity of helium to measure absolute viscosity values with similar standard uncertainty for other gases. In this case, only nominal measurements of the capillary radius r and length L were required; those values were used in the calculation of small corrections, and the value of L was used in the prefactor. With these results in mind and based on the principle that gas viscosity-ratio measurements are more accurate than absolute measurements, May *et al* [14] modified the two-capillary viscometer and applied the ratio measurement approach. The reference viscosity of helium at zero density and temperature at 298.15 K, $\eta^{\mathrm{He}}_{0,298}$, deduced from the best experimental data and the best value calculated *ab initio* [13] was used. The acquired viscosity of helium from two capillaries viscometer was $\eta^{\mathrm{He}}_{0,298} = 19.842$ (7) μPa·s, which deviates by 0.08% from the reported *ab initio*

results $\eta^{\mathrm{He}}_{0,298} = 19.8253\ (2)$ μPa·s. In 2007, May *et al* [15] continued measuring ratio viscosities $\eta^{\mathrm{gas}}_{0,298}/\eta^{\mathrm{He}}_{0,298}$ for several gases at low densities in the temperature range from 200 K to 400 K using a two-capillary viscometer with an uncertainty ranging between 0.024% and 0.077%. In 2012, Berg and Moldover [16] reviewed viscosity ratios near 298.15 K and zero density for 11 gases obtained with 18 instruments. They recommended new values with maximum relative standard uncertainties ranging from 2.7×10^{-4} to 3.6×10^{-4} at a 68% confidence level using the viscosity of helium calculated *ab initio*. Later in 2014, Berg *et al* [17] reviewed single-, two-, and four-capillary viscometers, and further recommendations for measurements at high-pressure conditions and of liquids were suggested based on the ratio measurements.

In 2016, a new equipment based on the capillary tube was developed for accurate high-pressure viscosity measurements. This equipment was designed based on the capillary flow technique and vibrating tube method, respectively, for viscosity and density measurements. The experimental results showed its capability of operating up to 70 MPa, with relative combined expanded viscosity uncertainties ranging from 0.07% to 4% [18].

In another research group, an in-house capillary tube apparatus was employed for viscosity measurements of CO_2-rich mixtures within the temperature range of 280 K–343 K and pressures up to 40 MPa. In this study, a stated uncertainty of 1% was reported, although only the uncertainty in pressure measurements was considered [19]. Subsequently, utilizing the same apparatus, the pressure range was expanded, enabling viscosity measurements at pressures up to 155 MPa. These measurements were conducted across various temperatures, ranging from 243 K to 423 K to cover the gas, liquid, and supercritical regions [20].

In 2015, a two-capillary viscometer was introduced based on principles described in [17]. In that work [21], viscosity measurements of liquid cyclohexane and decane were conducted between 303 K and 598 K, at pressures up to 4 MPa, with a 3.0% Additionally, the temperature range of the viscometer was extended to encompass viscosity measurements of liquid hexadecane at a temperature range of 323 K–673 K, and at pressures up to 4.0 MPa, maintaining the same uncertainty as in the previous work [22].

As discussed above, several publications have highlighted the potential for viscosity measurements achieving low uncertainty through viscosity ratio measurements involving two-capillary viscometers and *ab initio* calculations. Hence, the goal of this research work was to design and construct a modified two-capillary system to measure the viscosity of pure and mixed gases with lower uncertainty, applying the underlying principles introduced by Berg and Moldover [16].

2. Experimental methodology

The measuring principle of capillary viscometers is based on Hagen–Poiseuille equation because the roles of viscosity and flow rate are interchangeable. For a compressible fluid that flows through a capillary tube with a radius of r and length L, the flow rate with the ideal gas assumption yields:

$$\dot{n}_0 = \frac{\pi r^4 \left(P_{\mathrm{in}}^2 - P_{\mathrm{out}}^2\right)}{16L\,\eta^{\mathrm{gas}}(T,0)\,R_{\mathrm{gas}}T} \tag{1}$$

where R_{gas} is the universal gas constant and $\eta^{\mathrm{gas}}(T,0)$ is the viscosity of ideal gas in the limit of zero-pressure, and P_{in} and P_{out} are the pressures at the inlet and outlet of the capillary, respectively. The capillary impedance Z is given by [14]:

$$Z(T) = \frac{16L_T}{\pi r^4(T)}. \tag{2}$$

To compensate for the assumptions for the basic Hagen–Poiseuille equation, as explained in [23, 24], Berg [11] implemented several correction terms. With these corrections, the accurate hydrodynamic model for compressible fluids flowing through a capillary wound into a coil is in the form of:

$$\begin{aligned}\dot{n} = \dot{n}_0 \Bigg[& 1 + g_{\mathrm{virial}}(P_{\mathrm{in}}, P_{\mathrm{out}}) + 4K_{\mathrm{slip}}\mathrm{Kn} + \frac{K_{\mathrm{ent}}}{16}\frac{r}{L}\mathrm{Re} \\ & + \left(\frac{K_{\mathrm{exp}}}{8} + \frac{K_{\mathrm{thermal}}}{16}\right)\frac{r}{L}\mathrm{Re}\ln\left(\frac{P_{\mathrm{out}}}{P_{\mathrm{in}}}\right)\Bigg] f_{\mathrm{cent}}(\mathrm{De},\delta) \\ = \dot{n}_0 & \left(1 + \sum_{i=1}^{5} c_i\right) f_{\mathrm{cent}}(\mathrm{De},\delta) = \dot{n}_0 C^{\mathrm{gas}}(T, P_{\mathrm{in}}, P_{\mathrm{out}}).\end{aligned} \tag{3}$$

The three main factors in the expression for molar flow $\dot{n}$ are: (1) $\dot{n}_0$: the flow rate for an ideal gas, determined from equation (1), (2) five dimensionless correction terms in the bracket, will be further explained. (3) f_{cent} factor: correcting for the centrifugal effect due to curving the capillary into a coil.

Five dimensionless correction terms in the bracket include: (A) departures from the ideal gas behavior; g_{virial}. However, this term is valid only for high pressure gases and a different approach is needed for the liquid phase. (B) slip at the capillary walls; K_{slip}, (C) kinetic energy changes at the capillary entrance; K_{ent}, (D) gas expansion along the length of the capillary which increases the kinetic energy, causing additional pressure drop; K_{exp}, (E) thermal or radial temperature distribution along the capillary; K_{thermal} A detailed description of correction terms A–E and the model proposed for f_{cent} can be found in [12]. Here Kn, Re, De, and δ are Knudsen number, Reynolds number, Dean number and the ratio of the internal radius r of the capillary to the radius of coil, R_{curve}, respectively. For Poiseuille gas flow, the average pressure along the capillary:

$$\bar{P}_{\mathrm{in/out}} = \frac{2}{3}\left(\frac{{P_{\mathrm{in}}}^3 - {P_{\mathrm{out}}}^3}{{P_{\mathrm{in}}}^2 - {P_{\mathrm{out}}}^2}\right). \tag{4}$$

The ratio viscosity measurements can be performed more accurately than absolute viscosity measurements since the

impact of capillary geometry on the uncertainty of the measurements is cancelled out in the ratio equation. The working equation proposed by May *et al* [14] for high densities applying ratio viscosity measurement approach and using helium as reference fluid yields:

$$\eta^{\text{gas}}_{0,T} = \eta^{\text{He}}_{0,298}\left(\frac{\eta^{\text{He}}_{0,T}}{\eta^{\text{He}}_{0,298}}\right)_{ab\ initio}\left(\frac{\eta^{\text{gas}}_{0,298}}{\eta^{\text{He}}_{0,298}}\right)R^{\text{gas, He}}_{T,298} \tag{5}$$

where:

(1) $\eta^{\text{He}}_{0,298}$ is the viscosity of helium at zero density and reference temperature of 298.15 K calculated using *ab initio* [13] from quantum mechanics and statistical mechanics with uncertainty less than 0.01%.
(2) $(\eta^{\text{He}}_{0,T}/\eta^{\text{He}}_{0298})_{ab\ initio}$ is the temperature-dependent ratio for helium at 298.15 K and desired temperature T. Calculated *ab initio* [13] with uncertainty less than 0.01% in the range 200 K $< T <$ 400 K.
(3) $(\eta^{\text{gas}}_{0,298}/\eta^{\text{He}}_{0,298})$ is a reference value for the viscosity ratio, measured at 298.15 K. This ratio can be determined using a downstream capillary as a single capillary viscometer once for fluid under test and once for helium. Using a single capillary viscometer demands flow measurement.
(4) $R^{\text{gas, He}}_{T,\,298}$ is the measurement of the temperature-dependent ratio of viscosity ratios using the two-capillary viscometer. The $R^{\text{gas, He}}_{T,\,298}$ defines as:

$$R^{\text{gas, He}}_{T,298} = \left(\frac{\eta^{\text{gas}}_{0,T}}{\eta^{\text{gas}}_{0,298}}\right) \Big/ \left(\frac{\eta^{\text{He}}_{0,T}}{\eta^{\text{He}}_{0,298}}\right). \tag{6}$$

3. Experimental infrastructure

The two-capillary viscometer was designed in accordance with the principles of viscosity measurements described in [14, 17]. The two-capillary viscometer principle is based on the measurement of the pressure drop across the upstream capillary, which is proportional to the viscosity at the test temperature and pressure. The pressure drop over the downstream capillary at reference conditions is approximately proportional to the mass flow. The flow is gravimetrically calibrated with a separate custom-made setup. The main difference compared with previous works is the new design of the capillary configurations. The new configuration employs a total of 2 × 2 coiled capillaries with different inner diameters. Another difference is that the upstream capillary is used for the viscosity measurements and the downstream capillary for the flow measurements. The new facility can conduct measurements of viscosity and density in liquid, supercritical or gaseous states, with design temperatures between 213.15 K and 473.15 K and pressures up to 100 MPa. For the purpose of a detailed description, the rig has been divided into 12 sub-sections. A simplified schematic of the two-capillary viscometer comprising sub-sections E-01 to E-11 is shown in figure 1.

E-01: The gas supply (pure/mixture) provides the system with the pure or mixed gas from gas cylinders. Mixed gases with desired purity are prepared gravimetrically in house.

E-02: The high-pressure delivery system includes a syringe pump (PMP-1) to provide high pressure and regulate the desired pressure at the inlet of the capillaries (P_1). The pump is connected to a buffer volume tank for faster pressurization and stabilization of the upstream pressure and (P_5) can measure the pressure of pump and at the inlet of system controlled by PMP-1.

E-03: A commercially available vibrating tube densimeter integrated with the viscometer and enabling density measurements at the same temperature and pressure as the viscosity measurements.

E-04: Upstream capillary system contains viscosity capillaries (capillary 1 and capillary 2, alternatively) at high pressure in a thermostatic bath at the test temperature.

E-05: Downstream capillary system contains the reference capillary (capillary 3 and capillary 4, alternatively) at reference pressure in a thermostatic bath, normally at reference temperature.

E-06: Pressure reduction system that allows reduction of the high pressure in the upstream capillaries to the low pressure at reference capillary. This system includes a commercial actuator valve (V-26), the shut-off valves and small capillary coils.

E-07: High pressure measurement system consisting of two pressure transmitter arrays used to measure the input (P_1) and output (P_2) of capillaries 1 and 2, covering the full pressure range of the system.

E-08: Low pressure measurement system composed of two pressure sensor arrays P_3 and P_4 used for the capillaries 3 and 4 at low pressures.

E-09: A sphere-shaped tank and a scale for mass flow measurements. The methodology used to determine the fluid viscosity depends on accurate mass flow measurement via the pressure drop of the reference capillaries (3 and 4), which is calibrated upstream from the reference by gravimetric means.

E-10: The outlet of reference capillaries is connected to the vent. This system is designed to regulate pressure at outlet of

reference capillary (capillary 3 and capillary 4, alternatively) using a variable leak valve (V-35).

E-11: Vacuum pump integrated to the leak valve to control pressure P_4.

E-12 Separate vacuum system including pre-vacuum and high vacuum pumps. Several places (E-02, E-03, E-06, E-07, E-08) are connected to E-12 allowing for rapid evacuation of the entire system. E-12 is not shown in figure 1.

4. Overview of apparatus design and operations

As it can be seen in figure 1 the apparatus consists of several different parts. The following sections will discuss in detail the functions of the main parts of the setup: (1) capillaries design and configuration. (2) High pressure gas source. (3) Pressure and flow control. (4) Pressure measurements. (5) Temperature control. (6) Temperature measurement. (7) Mass flow measurements. (8) Density measurement.

4.1. Capillaries design and configuration

The capillary tubes are the core components of the two-capillary viscometer. The capillary tubes used in this work, called Polymicro capillaries, are made of fused silica glass and coated with polyimide outer surface for mechanical protection. In total, four Polymicro capillaries were used in the new design of the two-capillary viscometer with a new design of (2 × 2) capillary configurations. The new (2 × 2) configuration means that two pairs of capillaries are placed in sequence, i.e. two coiled capillaries downstream of two other coiled capillaries upstream, as illustrated in figure 2. However, during operation, only a single capillary at the upstream and a single capillary at the downstream are used simultaneously. The (2 × 2) configuration is one of the different features when compared to the two-capillary setups in previous works. All four coiled capillaries have the same outer diameter, of 794 μm with coating, but different inner diameters. Therefore, using different combinations of four capillaries enables the viscosity measurements with a wide range of flow rates at different temperatures and pressures. Upstream capillaries (1 and 2) with an inner diameter of 75 μm and 200 μm are used for the viscosity measurements at specified measurement conditions. In comparison, the two downstream capillaries (3 and 4) have an inner diameter of 250 μm and 500 μm and are used for the flow measurements at a reference temperature and pressure (298.15 K, 0.1 MPa).

The ends of the glass capillaries had to be connected to the rest of the setup for the fluid to enter from one end and exit from the other. The small inner diameter of the capillaries and the glass material made it challenging to fit them into the remaining equipment. Therefore, the capillaries' ends were augmented by metal sleeves, as seen in figure 3(a). The metal sleeves were glued with epoxy to the capillaries ends using a low-vapor-pressure epoxy (EP42HT-2 from Master Bond Inc) and connected to a T-piece, as seen in figure 3(b).

To avoid leakage in the capillary's interconnections, as anywhere in the setup, leakage tests were performed. Leakage tests were carried out at pressures up to 100 MPa and temperatures between 293.15 K and 423.15 K. The expansion coefficient of the metal sleeves is much higher than the glass capillaries. To avoid the leakage from the space between the capillary walls and metal sleeves, the gluing procedure was improved. An extra glue layer was applied on the outer surface of two edges, where the connection between capillary and metal sleeves starts and ends as shown in figure 3(a). The eight ends of four capillaries were glued to the metal sleeves, fitted to a stainless-steel T-piece through the ferrule fittings. The fluid enters or exits from the second arm of the T-piece. The ends of capillaries attached to the metal sleeves formed a least 10 cm straight length to direct fluid to the same height of the T-piece. The pressures at the inlet or outlet of the capillary are measured from the third arm of T-piece connected to the pressure system. The two capillaries of each system upstream or downstream are mounted around a stainless-steel grid, bent into a circular shape, as seen in figure 4, because the long capillaries were coiled several times. To secure the capillary position, particularly at high pressures, the capillaries were supported from abrasion by PTFE-coated thin wire to the stainless-steel grid in several places. The metal grid has a diameter of 0.5 m with a height of 0.15 m. Both metal grids (one at the upstream and one at the downstream) with the coiled capillaries around were horizontally mounted in a container, named inner tanks. The inner tanks are filled with the thermostatic fluid supplied from the thermostatic baths to control the temperature of the capillaries. It is important to increase the heat transfer inside the inner tank to ensure that the capillaries reached the target temperature within the desired time frame. Therefore, a heavy metal core was installed at the center of the space inside the inner tank with fiber pieces surrounding the capillaries to ensure turbulent flow resulting in higher heat transfer. An aluminum base plate with small holes was mounted horizontally to support the metal grid inside the tank and make an even flow of thermostated fluid in the inner tank. The temperatures of the capillaries are measured and controlled using multiple high-precision platinum resistance thermometers (PRTs) in the baths.

4.2. High pressure gas supply and upstream pressure control

The pure or mixed gaseous fluid is supplied from gas cylinders placed in a vented cabinet located in the same room as the viscometer. In the case of mixtures, due to the difficulty to find gas mixtures with desired low uncertainty in composition, mixed gases are prepared gravimetrically from CO_2-Mix facility of SINTEF [25]. Although the rig can be pressurized from the gas cylinder, the upstream pressure needs to be precisely regulated during the measurements using a pressure gauge. Thus, the gas cylinder is connected to a high-pressure syringe pump with maximum 50 ml volume (TOP-industry, PMHP model: 50–1000). The syringe pump pressurizes the system and regulates the upstream pressure P_1. A buffer tank with a volume of 120 ml is used immediately downstream of the

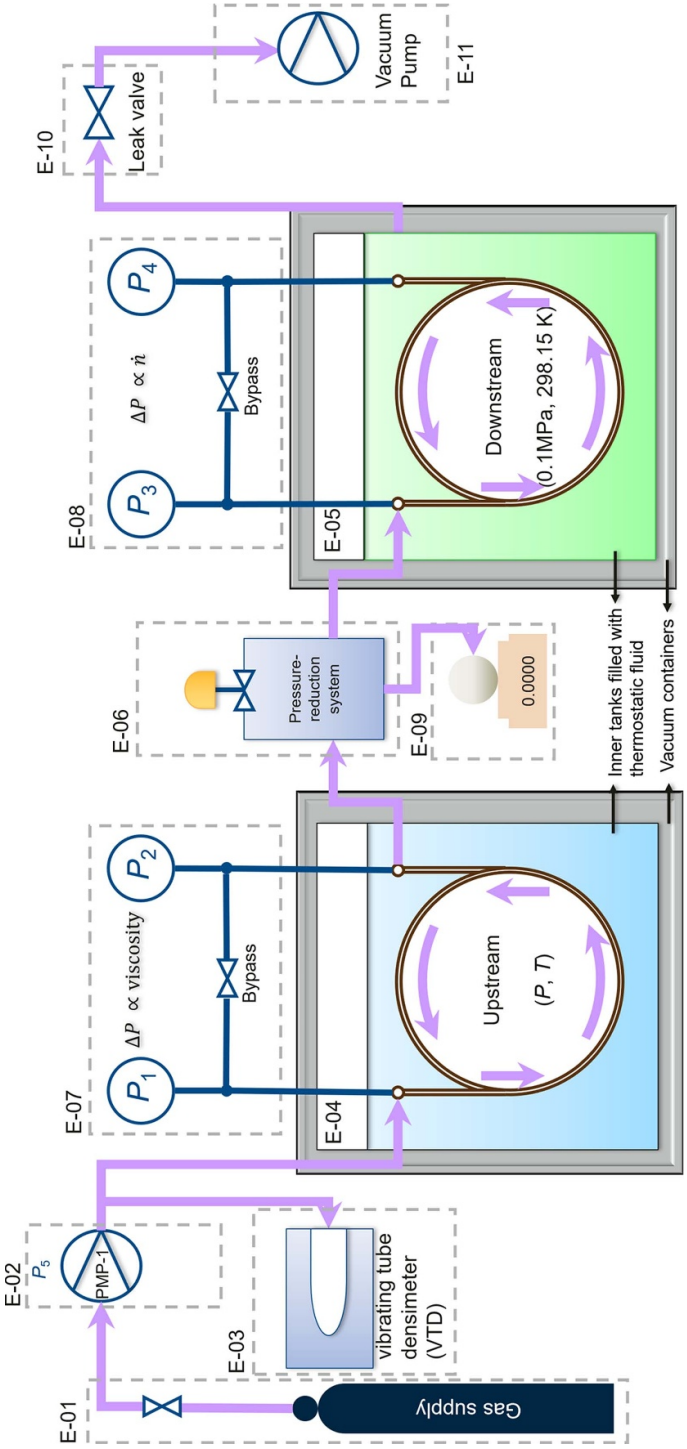

Figure 1. Simplified schematic of the two-capillary viscometer comprising sub-sections E-01 to E-11.

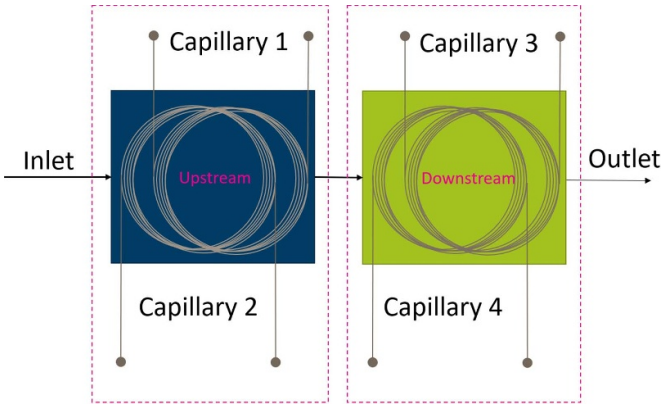

Figure 2. Simplified schematic of (2 × 2) coiled capillaries with the two upstream coils and two reference coils.

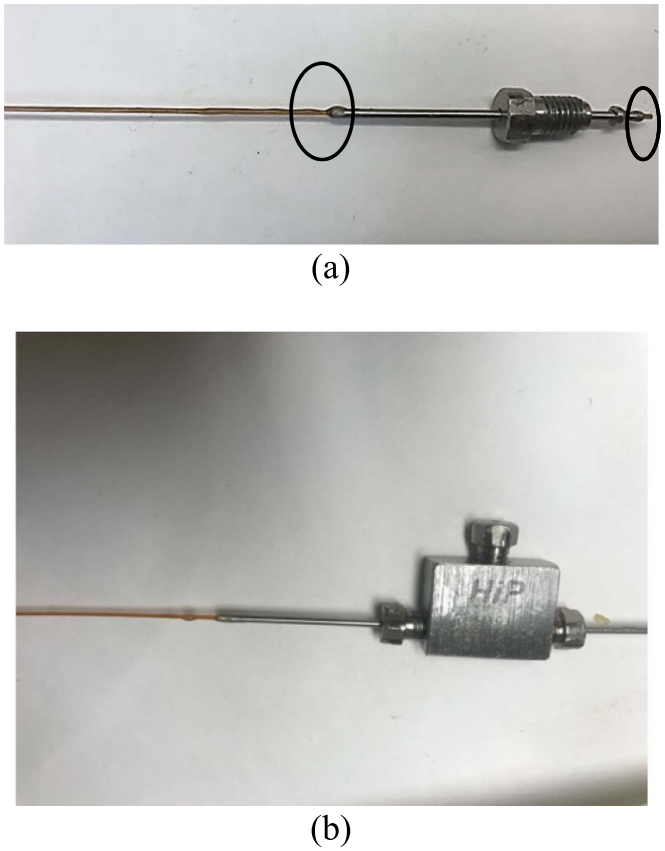

Figure 3. (a) Augmented end of a capillary by metal sleeves. The circles show the areas with extra gluing on the outer surface. (b) Capillaries end connected to a T-piece.

pump to stabilize the upstream pressure. The pressure of the pump, P_5, is measured using a Keller pressure transmitter with 100 MPa full scale (series 33X), 0.05% expanded uncertainty ($k = 1.73$). Several shut-off valves direct the fluid with the target pressure into the upstream capillary, either capillary 1 or 2, and the densimeter. To protect the capillaries from the particles and dust, a particle filter was installed after the buffer tank and before the inlet of the upstream capillaries. Figure 5 shows the position of inlet and outlets of capillaries, pressure and temperature sensors used in the rig.

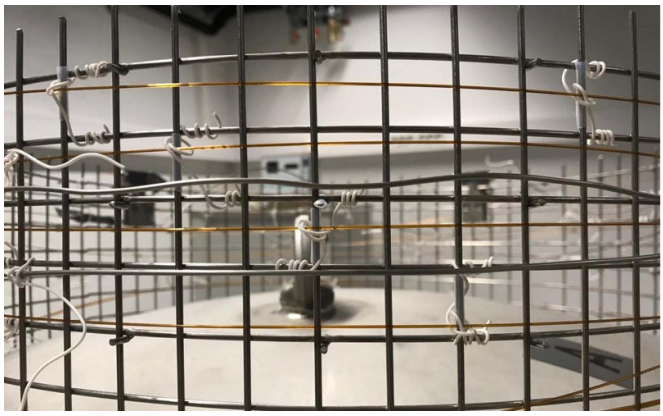

Figure 4. Coiled capillaries around the metal grid.

4.3. Pressure and flow control

Based on the Hagen–Poiseuille equation, the viscosity of a fluid is approximately proportional to the pressure drop of upstream capillary ($\eta \propto \Delta P_{\mathrm{up}}$) and inversely proportional to the flow rate ($\eta \propto 1/\dot{n}$). The flow rate is also a function of the pressure drop at the downstream capillary since the downstream capillary acts as a flow meter. Therefore, one can write that $\eta \propto (\Delta P_{\mathrm{up}}/\dot{n}) \propto (\Delta P_{\mathrm{up}}/\Delta P_{\mathrm{down}})$. The pressure drops along the upstream and downstream capillaries are $\Delta P_{\mathrm{up}} = P_1 - P_2$ and $\Delta P_{\mathrm{down}} = P_3 - P_4$. The pressure drop along the downstream capillary corresponds to a flow rate that can be calculated through a separate calibration.

A sophisticated pressure control system was employed to control the pressure and flow with high accuracy and stability. Three out of four pressures need to be controlled; the pressure P_1 at the inlet of the upstream capillary is controlled by the high-pressure syringe pump. The novel pressure-reduction system, E-06, regulates the pressure P_3 at the inlet of the downstream capillary. The pressure at the outlet of the downstream capillary P_4 is controlled using a variable leak valve (VAT Series 590), V-35, connected to a vacuum pump. The crucial pressure P_2 at the outlet of the upstream capillary is an unknown output and it is measured without regulation. P_2 together with P_1 provides the pressure drop ΔP_{up} through the upstream capillary for the viscosity measurements. As mentioned, E-06 was designed to control P_3. The upstream capillary operates at pressures up to 100 MPa, while the maximum pressure at the downstream capillary is at a reference pressure (usually below 0.2 MPa). No commercial control valve was found in the market to compensate for this large span of pressure differences and flow rates. This challenge required a custom-made cascade system consisting of six pneumatic shut-off valves, five small capillaries (Cap. 21-Cap.25) with high flow resistance, and an actuated variable/control valve, V-26, as illustrated in figure 6.

Part of the cascade system consisting of the small capillaries is operated to reduce the pressure to below 40 MPa before valve V-26. In this design, the shut-off valves (V21–V25) are

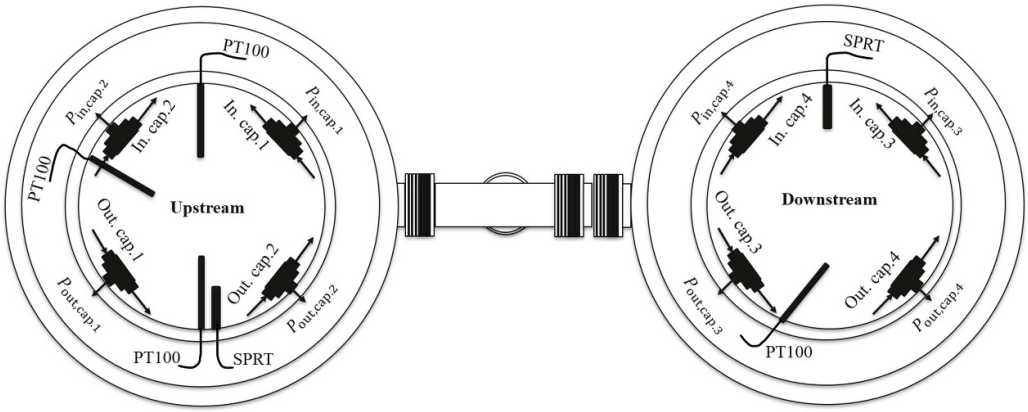

Figure 5. Interior of upstream (E-04) and downstream (E-05) containers from topside.

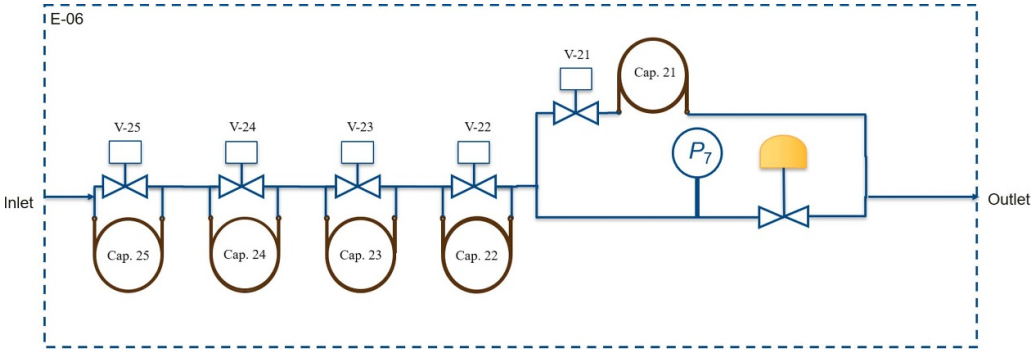

Figure 6. A simple sketch of pressure-reduction system (E-06).

closed or opened depending on the upstream pressure and flow. The valves direct the flow through a selection of capillary coils to provide high scalability in flow resistance. The small capillaries are similar to the capillaries used in the rig, but with different geometric parameters. That is, the outer diameters of these five capillaries are 363 µm, the inner diameters vary between 25 µm and 75 µm and lengths are up to 5 m. Hence, the high pressure at the end of the upstream capillary is reduced to the specified value of the pressure further down through the E-06.

The performance of valve V-26 was checked by a flow rate change of helium for given position from fully open position 100% to fully close position 0%. A high pressure of 10 MPa was induced upstream of valve V-26 and a desired pressure of 0.15 MPa downstream of V-26. Figure 7 shows the flow rate of helium when the position of the valve was set at different values. The outputs were recorded for at least 15 min. The results indicate an effective operating flow range between 10% and 70% valve opening. This means that for the positions below 10% the valve is almost fully closed and for the positions above 70%, the change in position does not change the flow and the valve is almost fully open. The valve characterization was crucial for the flow measurements. The valve showed a similar trend for different upstream pressures.

For very low-pressure measurements, a different valve configuration is required because V-26 operates in its fully open position and therefore cannot regulate the flow through the

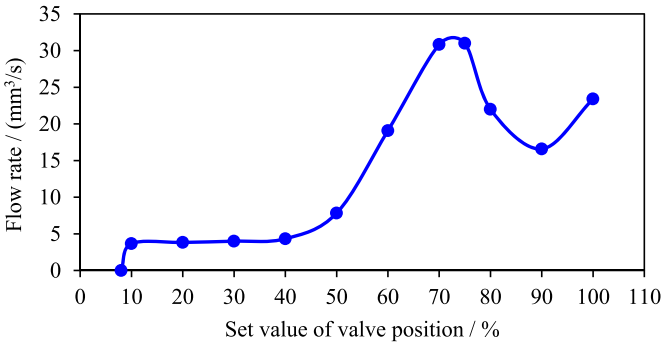

Figure 7. Flow rate of helium at the different set value for the position of V-26 at pressures 10 MPa upstream and 0.15 MPa downstream of V-26.

downstream capillary. However, by opening valve V-21 in figure 6 and using the capillary 21, V-26 can control the flow with a lower resistance to the pressure of P_3. The pressure in E-06, is measured right before V-26, using a Keller pressure sensor (series 35X, 0.1% expanded uncertainty) with the maximum pressure 40 MPa.

4.4. Pressure measurements

The pressure measurements at the inlet P_1 and outlet P_2 of the upstream capillary are performed using arrays of pressure

transmitters. The pressure sensors are placed in a custom-made box with air bath. The P_1 array mirrors that of P_2. Each side (P_1 or P_2) is comprised of a high precision Keller pressure transmitter with 100 MPa full scale (series 33X) and three pressure transducers manufactured by Paroscientific with Digiquartz electronics for pressures up to 14.8 MPa, 6.9 MPa, and 2.1 MPa. The quartz crystals inside the Paroscientific transducers generate two square wave signals with periods proportional to either the applied pressure or the internal temperature. The Digiquartz electronics then measure and integrate these signals over a specified timeframe to determine their periods. This integration time can be set between 0.001 s and 270 s in 0.001 s increments to adjust resolution and sensitivity. The pressure sensors also offer a parts-per-billion resolution with a standard uncertainty of 0.01%. The pressure sensors P_1 and P_2 with a total of eight pressure sensors are kept in an insulated box equipped with heating elements for the purpose of temperature control. The desired temperature for the pressure sensors depends on the critical temperature of the fluid. For example, for CO_2, 313.15 K is kept avoiding phase separation. For mixtures with other condensable components, higher temperatures might be needed. Similar to the upstream array, the P_3 array mirrors that of P_4 at the downstream and consists of two pressure sensors for a maximum pressure of 6.9 MPa and 0.21 MPa. Because the downstream capillary operates at a maximum pressure of 0.2 MPa, there is no need for a pressure transducer with a higher-pressure rating. The pressure sensors at the upstream and downstream are kept in separate boxes for better temperature control. This assortment in full-scale pressures takes advantage of more precise low-pressure measurements and are suitable for corrosive fluids.

The pressure transmitters are protected from excessive pressures by automatic closing valves. In case there is a malfunctioning of this protective system, rupture discs (pressure safety discs) protect the pressure transmitters. Gas lines are kept in insulated boxes or warmed by heating elements for temperature control. As illustrated in figure 1, there are two actuated bypass valves between the inlet and outlet of capillaries connected to the pressure measurement system, one at the upstream and one at the downstream. The bypass valves are open before and after each measurement at a given pressure to measure the pressure difference between the pressure readings at the entry and exit pressure sensors, called bias measurements. The bias measurements are recorded when there is no flow in the capillaries and the pressure is stabilized. In that way, the zero-point drift of the sensors due to the deviations from the calibrations, temperature difference, hydrostatic pressure or other sources can be assessed. Consequently, very accurate pressure difference measurements are possible.

4.5. Temperature control

Both dynamic and kinematic viscosities are sensitive to the temperature deviations. To obtain accurate values for kinematic viscosities, good temperature control is important to avoid additional uncertainty during measurement. As mentioned, the capillaries are placed in the inner tanks immersed in the thermostatic fluid. To ensure that the fluid reaches the target temperature at the inlet of the capillary, the fluid first enters into a stained steel tubing with 25 mm diameter after 1 and 3/4 turn around the metal grid to equalize the temperature. Afterwards, the heated/cooled fluid enters the inlet of the capillary. The thermostated liquids were provided from two Julabo thermostatic circulators with different temperature ranges. The Julabo baths provided a stability of 0.02 K–0.2 K, which was an insufficient stability compared to what was desired. Therefore, the baths were combined with heating elements before the thermostatic tanks.

The Julabo baths specifics: (1) Model FP89-HL is an ultra-low refrigerated-heating circulator for the low-temperature range of 213 K–373.15 K, with temperature stability of $\pm$0.02 K and cooling power of 0.58 kW at 213 K. Ethanol is used below its flash point temperature. For higher temperatures, water or silicone oil is used. (2) Model MA-12 is a pure heating circulator for the higher temperature area of 293.15 K–423.15 K with temperature stability $\pm$0.01 K and water or silicon oil as working fluids. (3) For temperatures near or below ambient temperature, the MA-12 has an integrated connection for tap water to provide additional cooling power. The design of temperature system required filling the upstream and downstream tanks and pipes with approximate 60 l of thermostatic fluid.

Both circulators control the temperature of the thermal fluids independently. They measure the temperatures from their respective containers and control them depending on the desired value with integrated PID controllers. The temperature control system includes high-temperature and low-temperature circulators, and a cooling water circuit. Several valves are implemented to evacuate air from the system. To switch the thermostatic fluids, the respective pipes had to be drained and cleaned first. The cleaning is performed manually. Therefore, the displayed valves are all manually operated. The temperature control system uses the low-temperature circulator for a cold cycle and high-temperature circulator for a warm cycle with its internal pumps. The circulators' temperatures are controlled using PT100 sensors integrated with the baths. Since internal pumps could not deliver the necessary mass flow of 0.6 kg s^{-1} required for the desired thermal uniformity, external pumps were installed for each circulator. Furthermore, electrical heaters and temperature sensors are components of the temperature control system. A pump and a tank for storage of the fluid are implemented to enable drainage of the system. The electrical heaters were used to reduce oscillations in temperature. Therefore, the two-temperature sensors were placed after the electric heaters to detect any temperature deviations. Because it is necessary to cover the whole temperature range, the working fluid needs to be exchanged occasionally. Therefore, a drainage system was designed.

The operation of the temperature control system is split into four different modes of operation: (1) the high-temperature circulator controls the measurement container, and the low-temperature circulator controls the reference container. (2) The high-temperature circulator controls the reference container, whereas the low-temperature circulator controls the measurement container. (3) The high-temperature circulator

controls both containers. (4) The low-temperature circulator controls both containers.

All the pipes used in the temperature control system were covered with the insulation materials (Armaflex foam insulation at low and fiberglass at high temperatures). As mentioned earlier, the capillaries were immersed in the thermostatic containers inside an inner tank. The inner tanks were placed inside the vacuum insulated outer tanks. The inner tanks were covered with two different types of insulation (ten layers of aluminum sheets and six layers of aluminum coated plastic).

4.6. Temperature measurements

The temperatures in the containers are measured by several PRTs. At upstream capillary, a SPRT (25 Ω Standard PRT) for very high accurate measurements and three PT100s are used to investigate uniformity and stability. The SPRT and one PT100 are installed at the bottom of the inner tank and two PT100s at the top to check the uniformity of temperature as well. Since the downstream capillary operates at the reference temperature of 298.15 K, except for the helium calibrations, only one SPRT at the bottom and one PT100 at the top are used. The SPRTs were manufactured by FLUKE and are specified for a temperature range of 13.15 K–505.15 K with a resistance of 25.5 Ω at 273.15 K and a stability of 0.001 K. The PT100s are specified from 73.15 K to 1073.15 K with a standard uncertainty of 0.01 K.

4.7. Mass flow measurements

The viscosity measurements are dependent on the flow rate. In the two-capillary viscometer, the downstream capillary operating at the reference conditions acts as a mass flow meter. However, the flow rate requires separate calibration. For this purpose, a custom-made gravimetric setup was designed for the mass flow gravimetrically calibrations. An empty sphere filled with a certain amount of fluid (maximum 4 MPa) is connected to the downstream capillary, as shown in E-09 in figure 1. A constant mass flow runs from a sphere into the downstream capillary. The pressure at the inlet and outlet are kept constant at the predetermined values and reference temperature. The duration of the mass flow experiment is the time that constant pressures are maintained and stable. The mass flow rate is calculated by weighing the sphere with fluid content before and after the flow experiment. In order to reduce the impact of various error sources, such as buoyancy and non-ideal repeatability/linearity of the scale, an ABBA scheme with a comparator is used [25, 26]. The principle depends on comparing the object to be weighed (A) with a calibrated reference mass (B) by alternatingly placing the two objects on the comparator.

4.8. Density measurements

A densimeter is integrated into the setup to measure the density at the same temperature and pressures as the viscometer. An integrated densimeter allows for the accurate conversion between kinematic and viscosity. The density meter is a commercial device, DMA HPM (oscillating tube), manufactured by Anton Paar. The density meter conducts the density measurements for a temperature range of 263.15 K–473.15 K and pressures up to 100 MPa, which has a standard uncertainty between 0.1 mg cm^{-3} and 1 mg cm^{-3} (223.15 K with higher uncertainty). The principle of the density measurement is to measure the resonance frequency of the fluid-filled tube. An oscillating tube is excited to vibrate as the sample is introduced into the density meter. A mathematical conversion is then required for the precise determination based on the corresponding frequency to the density of the sample [27].

5. Design parameters

5.1. Capillary specifications

The geometrical parameters of the capillaries, including the inner radius (r) and length (L), were estimated based on the initial analysis of mass and volume flow, pressure drop, Dean and Reynolds numbers for the design temperature range of 213 K–473 K, and pressure range up to 100 MPa. Optimum geometrical parameters were estimated based on the feasibility and the target uncertainty of the measurements. For example, the glass capillaries with the outer diameter of 794 μm needed a minimum bending radius of 0.240 m. The target for relative uncertainty in viscosity was 0.03% for CO_2, except close to the critical point. The uncertainty in the flow increases as the diameter of the capillary is reduced due to slip on the wall [11].

The geometrical parameters were mainly estimated for CO_2 and helium but can be applied to fluids with the same order of kinematic viscosity as well. The lengths of the capillaries are in the order of a few meters to fulfill the criteria of the hydrodynamic model (ratio of r/L must be small enough). The long capillaries are winded into several coils to keep them in a smaller space and for easier temperature control. Table 1 presents the optimal inner radius and length of capillaries and the number of coils.

5.2. Dean number

Coiling the capillaries results in a reduction in the molar flow rate. In fact, curving the capillary creates a secondary transverse flow. Larrain and Bonilla [28] presented a model to determine f_{cent}, which yields an uncertainty of 0.02% for flow when $\text{De} \leqslant 16$, where Dean number definition can be found in [12]. In general, geometric imperfections of the capillaries cannot be characterized precisely, but they can impact the uncertainty of the centrifugal effects on the flow. Using quartz capillaries and operating at small Dean number decrease the effects of variation in the radius along the length of the capillary and the impact of the ellipticity on the flow. May *et al* [14] used a relative error due to flatness ε of an ellipse:

$$\frac{\Delta P_{\text{cent}}}{\Delta P} \approx K\varepsilon \text{De}^4 \tag{7}$$

Table 1. Optimal number of coils and lengths for the capillaries.

Parameters	Symbol	Capillary 1	Capillary 2	Capillary 3	Capillary 4
Inner radius/μm	r	37.5	100	125	250
Number of coils around grid	N	8.5	7.5	4.5	5.5
Capillary length/m	L	13.22	11.67	7.00	8.56
Coil curvature radius/m	R_{curve}	0.25	0.25	0.25	0.25
Capillary impedance/μm^{-3}	Z	34.059	0.594	0.146	0.011

The uncertainties of ±12 μm and ±6 μm (except ±3 μm for capillary 1) were reported by the manufacturer for the outer diameter and inner diameter of capillaries, respectively. The uncertainties of lengths are ±0.010 m.

where K is a 'constant given by the theory' [14]. The presence of unavoidable eccentricity errors leads to a maximum in the allowable Dean number:

$$\mathrm{De}_{\max} \approx \left(\frac{\left(\frac{\Delta P_{\text{cent}}}{\Delta P}\right)_{\max}}{K\varepsilon} \right)^{\frac{1}{4}}. \tag{8}$$

Berg [12] estimated the flatness of $\varepsilon = 0.01$, which gives $K = 3 \times 10^{-6}$. With a target error contribution of 0.03% uncertainty in this work as well, we have:

$$\mathrm{De}_{\max} \approx \left(\frac{3 \cdot 10^{-3}}{3 \cdot 10^{-6}\varepsilon} \right)^{\frac{1}{4}} = \left(\frac{100}{0.01} \right)^{\frac{1}{4}} = 10. \tag{9}$$

In practice, smaller ellipticity errors than $\varepsilon = 0.01$ is expected for the glass capillaries used in this work [12].

5.3. Reynolds number

Reynolds number is a local quantity and depends on the locations z along the capillary. The Reynolds number must be determined to characterize the flow regime. Three correction factors K_{ent}, K_{exp} and K_{thermal} and the Dean number are dependent on the Reynolds number [12]. As discussed in table 1, the coil radius is 0.25 m, and the minimum inner capillary radius is 75 μm. Hence, the maximum Reynolds number yields:

$$\begin{aligned} \mathrm{Re}_{\max} &= \mathrm{De}_{\max}\sqrt{R_{\text{curve}}/r_{\min}} \\ \mathrm{Re}_{\max} &= 10\sqrt{0.25/\left(75 \times 10^{-6}\right)} = 577 \end{aligned}. \tag{10}$$

The maximum Reynolds number gives that the flow will always be in the laminar flow regime ($\mathrm{Re}_{\text{crit}} = 2300$) if the requirement of $\mathrm{De} < 10$ is fulfilled.

5.4. Other design considerations

The gradients in pressure, temperature and compositions of the fluid cause a change in the density of the fluid at different positions in the system. The height difference between pressure transducers at the inlet and outlet of the capillaries causes a gradient in pressure (bias) in the measurements due to the hydrostatic pressures. In theory, this error is detected or compensated for by the bias measurement between pressure sensors. Therefore, all pressure sensors were placed at the same height of inlet and outlet capillaries to obtain accurate measurements. The pipes from and to the tanks and pressure sensors were also kept at the same level.

Composition gradients in fluid mixtures could be significant. To avoid phase transitions all tubing is heated using the heating elements. Another solution is to perform the measurements in a suitable sequence (depends on the cricondenbar and cricondenterm, the maximum pressure and temperature, respectively, that vapor and liquid can coexist) to ensure that one stays outside the phase envelope. In general, such phase transitions are complex phenomena that could lead to variations in composition. Due to the very long length of capillaries compared with the diameter, the system is operating at steady state flow and the impact on the viscosity measurements is small. To reduce the impact of gradients in pressure and composition in the pressure measurement lines, the temperature of the E-07 is increased far above the critical temperature of CO_2. However, this may affect the temperature and pressure sensors stability and performance. The density gradients caused by temperature variations could affect the uncertainty of the measurements. For pure CO_2, temperature variation effects are much smaller than for various mixture compositions.

6. Results and discussion

6.1. Optimum flow rate

An optimum flow rate is necessary for accurate measurements. The main constraints on the flow rate comprised of: (i) the maximum flow is limited to the threshold of the laminar region, (ii) significant variations in fluid properties along the capillary must be avoided, (iii) high flow, and thus a large pressure drop, leads to an increasing impact of non-linearities in the viscosity and density of the fluid as a function of pressure, (iv) the maximum flow rate is limited by the Dean number (v) the minimum flow rate increases the uncertainty of the pressure measurements. Therefore, to estimate an optimum flow rate, the capillaries' geometry design parameters were carefully estimated for helium and CO_2. In this work, capillary 2 with an inner diameter of 200 μm at upstream and capillary 4 with an inner diameter of 500 μm at downstream were used. Different pressure drops/flow rates for helium as reference fluid were evaluated. In all cases, the average pressure at the downstream capillary was 0.1 MPa. The experiments showed that getting a stable pressure drop above 0.09 MPa

Table 2. The results of valve positions when different pressure drops tested in the downstream capillary where $T_{\text{ref}} = 298.15$ K. The upstream pressure P_7 was set at 3.5 MPa.

P_3/MPa	P_4 set/MPa	Actual P_4/MPa	V-26	V-35	$Z_{\text{down}}/Z_{\text{V35}}$	Feasibility
0.190	0.010	0.062	80%	80%	8.61	NP[a]
0.180	0.020	0.059	74%	80%	8.388	NP
0.170	0.030	0.056	73%	80%	8.245	NP
0.160	0.040	0.054	70%	80%	7.986	NP
0.150	0.050	0.051	66%	80%	7.920	NP
0.145	0.055	0.055	64%	67%	6.150	Possible
0.135	0.065	0.065	60%	66%	3.393	Possible
0.115	0.085	0.085	55%	65%	0.841	Possible

[a] Not possible.

Table 3. Mass flow calibration results.

Flow	Fluid	P_3/MPa	P_4/MPa	(P_3—P_4)/MPa	Duration/h	Mass difference/g	Mass flow rate/μg/s
High flow	He	0.145	0.055	0.090	3.06	1.3900	126.344
	CO_2	0.135	0.065	0.070	3.73	19.1019	1424.027
Low flow	He	0.115	0.085	0.030	14.72	2.2260	41.944
	CO_2	0.115	0.085	0.030	10.09	22.6776	615.552

was not feasible, as shown in table 2. Because at these conditions, the leak valve (V-35) operated in its fully open position (80%) and could not regulate the flow through the downstream capillary. An impedance ratio $Z = 16L/\pi r^4$ between the downstream capillary and the leak valve, connected to the vent (P_{vent}), is defined as:

$$\frac{(P_3 - P_4)\bar{P}_{3,4}}{(P_4 - P_{\text{vent}})\bar{P}_{4,\text{vent}}} = \frac{Z_{\text{down}}}{Z_{\text{V35}}} \tag{11}$$

The results show that the maximum impedance ratio resistance of 6.15 is corresponding to a pressure drop of $(P_3 - P_4) = 0.09$ MPa for helium.

6.2. Flow rate results

The downstream capillary was calibrated for the flow measurements. Table 3 summarizes the results of two different mass flow (high and low) calibrations for each fluid: helium and CO_2. The consistency between the mass flow measurement results was checked by repeating ten measurements for helium and resulting in a standard uncertainty of 0.06 μg s^{-1} the low flow. The repeatability was the main contribution to the uncertainty of the flow measurements. Finally, the relative combined uncertainties of 0.14% and 0.02% for helium and CO_2, respectively, were achieved. The low molecular weight of helium contributes to a proportionally higher uncertainty during the weighting and higher diffusivity of helium leads to elevated mass loss due to leakage.

In figure 8, the pressure drops of $(P_3 - P_4)$ were plotted over the mass flow rate. An auxiliary data point at zero was considered with this assumption that that the pressure drop is equal to zero when there is no flow through the capillary. The hydrodynamic model describes the flow well since the pressure drop and the mass flow rat, including correction factors explained in the next section, are linearly related, as shown in figure 8.

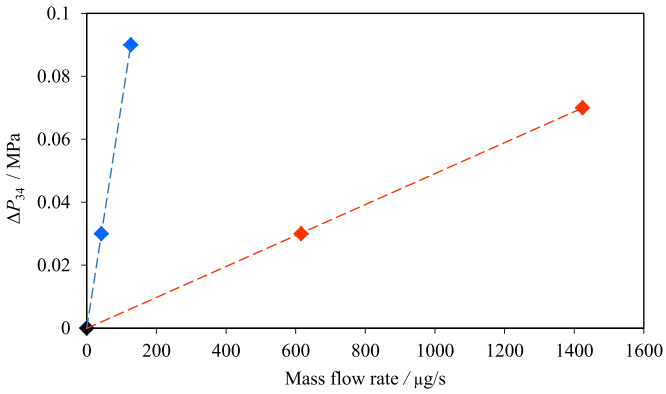

Figure 8. The pressure drop along the downstream capillary as a function of flow rate. The correction factors are included in the results. The marked data points are experimental data; helium (blue) and CO_2 (red). The dashed lines correspond to a linear fit.

6.3. Relative size of the corrections

Table 4 presents the correction coefficients used to determine the flow in equation (3) and effect of correction terms on the flows of 10.49 μmol s^{-1} helium and 13.99 μmol s^{-1} CO_2 at $T = 298.15$ K and $\bar{P}_{3,4} = 0.1$ MPa. The large correction terms arose due to the departures from the ideal gas behavior and the slip corrections for CO_2 and helium, respectively. The results for the flow of helium are consistent with the corrections for flow of 10 μmol s^{-1} of helium measured by Berg [12].

6.4. Reference viscosity ratio

The viscosity of CO_2 in the limit of zero density and the temperature of 298.15 K, $\eta^{CO_2}_{0,298.15} = 14.915$ μPa·s with the

Table 4. The correction coefficients used in this work and the effect of correction terms on the flows of 10.49 μmol s^{-1} helium and 13.99 μmol s^{-1} CO_2 at $T = 298.15$ K and $\bar{P}_{3,4} = 0.1$ MPa.

	Coefficient K		Correction term		% of $\dot{n}$	
	CO_2	Helium	CO_2	Helium	CO_2	Helium
g_{virial}	—	—	0.005 10	−0.000 66	0.51	−0.07
Slip	1.03	1.18	0.000 80	0.004 17	0.08	0.42
Entrance	−1.14	−1.14	−0.000 22	−0.000 01	−0.02	−0.001
Expansion	1	1	−0.000 15	−0.000 01	−0.01	−0.001
Thermal	−0.22	−0.32	0.000 01	0.000 001	0.001	0.0001
Centrifugal	—	—	0.999 96	1.000 00	−0.004	0.000

Table 5. Re-evaluated reference value, $\eta^{CO_2}_{0,298.15}$ in the limit of zero density.

Original reference	T/K	Re-evaluated value by [30]/μPa·s
Vogel and Barkow [32]	297.93	14.881 (10)
Hendl *et al* [32]	298.48	14.908 (3)
Schäfer *et al* [31]	298.152	14.888 (4)

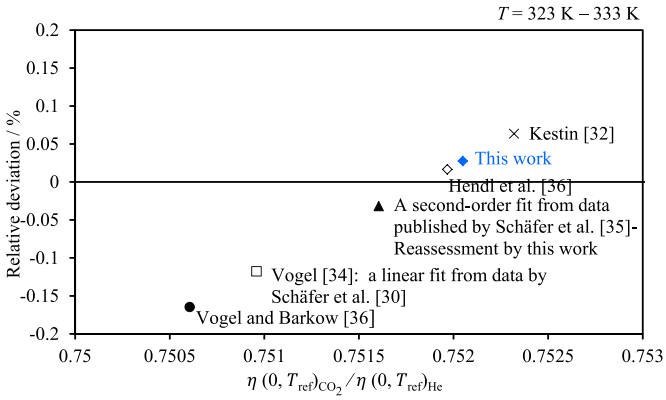

Figure 9. Deviations of various measurements from *ab initio* calculations of the viscosity of CO_2 at zero density. The baseline is the data from *ab initio* calculations [13, 33].

estimated standard uncertainty of ±0.1%, reported by Kestin *et al* [29]. However, Vogel [30] in 2016 evaluated the reported reference value $\eta^{CO_2}_{0,298.15} = 19.861$ μPa·s for helium by the same work, which differed from high accurate reference value for helium $\eta^{He}_{0,298.15} = 19.8253$ μPa·s, calculated by Cencek *et al* [13] with an uncertainty less than 0.001%. The result of 0.18% difference in the viscosity of helium questioned the validity of the reference value estimated by Kestin. Vogel [30] re-evaluated the reliable experimental viscosity data of dilute CO_2 measured by Schäfer *et al* [31] with a Taylor series based on temperature as the measurements had been performed in variable temperatures. The reference value $\eta^{CO_2}_{0,298.15} = 14.888$ μPa·s was achieved after extrapolation of the re-evaluated data in the range of 0.1 MPa–0.6 MPa with the uncertainty of 0.2%, expressed by a first-order series expansion in density. In addition, the viscosity data measure by [32, 33] were re-calibrated using the new reference value. The temperature and density dependencies of the viscosity of CO_2 were also considered in the re-evaluation since the measured points were not performed at 298.15 K and not at zero density [30]. Table 5 summarizes the results of re-evaluated reference value.

However, the linear extrapolation of experimental data by Schäfer [31] performed by Vogel [30] is questionable. Since the data show a polynomial trend, $\eta^{CO_2}_{0,298.15} = 14.900$ μPa·s from a second-order polynomial extrapolation was estimated in this work, agreed with the other existing data.

Furthermore, Hellmann [33] determined the reference viscosity of CO_2 using a four-dimensional intermolecular potential energy surface for two rigid CO_2 molecules determined from quantum-chemical *ab initio* calculations. The scaled theoretical value (by a factor of 1.0055), $\eta^{CO_2}_{0,T_{ref}} = 14.905$ μPa·s. A standard uncertainty of 0.2%, between 300 K and 700 K, and up to 0.55%, between 150 K and 2000 K. In 2017, a reference correlation [34] for the viscosity of CO_2 was developed based on compiling of comprehensive database of experimental and computed data. In the new correlation, a developed expression for the temperature dependence of $\eta_0(T)$ in the limit of zero density was employed. The expression of reference viscosity is based on the calculated *ab initio* by Hellmann [33] and is independent of the size, shape, charge distribution, and polarizability of a molecule, the length, and energy scaling parameters used in the kinetic theory. The expression is a scaled correlation with the seven adjustable parameters to match the calculated *ab initio* results with values derived from the most accurate experimental data. An uncertainty of 0.2% between 300 K and 700 K and 1% at between 150 K and 2000 K for $\eta^{CO_2}_{0,T_{ref}} = 14.905$ μPa·s was estimated. In this work, the reference value ratio $(\eta^{CO_2}_{0,298.15}/\eta^{He}_{0,298.15}) = 0.7524$ was measured. To compare the result of this work with the previous works, the viscosity of CO_2, $\eta^{CO_2}_{0,298.15}$, was taken from available literature data and the reference viscosity value for helium $\eta^{He}_{0,298.15} = 19.8253$ μPa·s was used to calculate the reference value ratio $(\eta^{CO_2}_{0,T_{ref}}/\eta^{He}_{0,T_{ref}})$. The calculated *ab initio* data for both CO_2 and helium were used as baseline. Figure 9 shows a positive relative deviation of less than 0.05% for the measured value of this work from the baseline. The deviation of the results of this work is the results of the high uncertainty of flow measurements for helium, but still comparable

to the uncertainty of *ab initio* calculations and uncertainty of the experimental data.

7. Conclusions

A two-capillary viscometer has been designed and built for measurements of viscosity of CO_2-rich mixtures relevant for CO_2 transport and storage. This article focuses on the construction of the facility and the processes for its operation, which could help other groups to construct a similar instrument. The viscometer enables to cover a wide range of between 213 K–473 K in temperature and up to 100 MPa in pressure. The crucial parameters such as length and radius of capillaries and coil curvature radius were estimated based on a target uncertainty of 0.03% in viscosity. Uncertainty analysis needed for the estimation of the measurement viscosity is also thoroughly described and the main contributions to the uncertainty of temperature, pressure, pressure drop, flow calibrations and leakage are identified. Two different flow rates were characterized for an average pressure of 0.1 MPa at downstream capillary based on the best performance of impedance of valves to control inlet and outlet pressures. The relative combined uncertainties of 0.14% and 0.02% for mass flow calibrations of helium and CO_2, respectively, dominate the other contributions to the uncertainty. The reference viscosity ratio $(\eta^{CO_2}_{0,298.15}/\eta^{He}_{0,298.15})$ was investigated in this work to validate the performance of the apparatus for the flow measurement. The observed deviation less than 0.03% is consistent with the data from accurate values calculated using *ab initio*. This value is also very close to the target uncertainty of this work. However, for the viscosity measurements at high pressures, it is expected that the uncertainty arises from the pressure drop will have a significant contribution budget. This requires further investigation at high pressures viscosity measurements.

Acknowledgments

This publication has been produced with support from the from the research program CLIMIT and the NCCS Centre, performed under the Norwegian research program Centers for Environment-friendly Energy Research (FME). The authors acknowledge the following partners for their contributions: Aker Solutions, ANSALDO Energia, CoorsTek Membrane Sciences, EMGS, Equinor, Gassco, KROHNE, Larvik Shipping, Lundin, Norcem, Norwegian Oil and Gas, Quad Geometrics, TOTAL, and the Research Council of Norway (257579/E20 and 280394)

ORCID iD

Anders Austegard https://orcid.org/0000-0001-9252-4618

References

[1] Munkejord S T, Hammer M and Løvseth S W 2016 CO_2 transport: data and models–a review *Appl. Energy* **169** 499–523

[2] Wang J, Ryan D, Anthony E J, Wildgust N and Aiken T 2011 Effects of impurities on CO_2 transport, injection and storage *Energy Proc.* **4** 3071–8

[3] Khosravi B, Betken B, Jakobsen J P, Løvseth S W and Span R 2022 Viscosity measurements of CO_2-rich; CO^{2+} N_2 and CO^{2+} H_2 mixtures in gas or supercritical phase at temperatures between 273 and 473 K and pressures up to 8.7 MPa *Fluid Phase Equilib.* **560** 113519

[4] Both J *et al* 2015 Gravity-driven convective mixing of CO_2 in oil *The Third Sustainable Earth Sciences Conf. and Exhibition* (EAGE Publications BV)

[5] Poiseuille J L 1844 *Recherches expérimentales sur le mouvement des liquides dans les tubes de très-petits diamètres* (Imprimerie Royale)

[6] Swindells J, Coe J Jr and Godfrey T 1952 Absolute viscosity of water at 20 C *J. Res. Natl Bur. Stand.* **48** 1

[7] Hoogland J, Van den Berg H and Trappeniers N 1985 Measurements of the viscosity of sulfur hexaflouride up to 100 bar by a capillary-flow viscometer *Physica* A **134** 169–92

[8] Kestin J, Sokolov M and Wakeham W 1973 Theory of capillary viscometers *Appl. Sci. Res.* **27** 241–64

[9] Wakeham W A 1991 Measurement of the transport properties of fluids *Experimental Thermodynamics* (Blackwell Science Ltd)

[10] Hunter I, Marsh G, Matthews G P and Smith E B 1993 Argon+ carbon dioxide gaseous mixture viscosities and anisotropic pair potential energy functions *Int. J. Thermophys.* **14** 819–33

[11] Berg R F 2004 Quartz capillary flow meter for gases *Rev. Sci. Instrum.* **75** 772–9

[12] Berg R F 2005 Simple flow meter and viscometer of high accuracy for gases *Metrologia* **42** 11

[13] Cencek W, Przybytek M, Komasa J, Mehl J B, Jeziorski B and Szalewicz K 2012 Effects of adiabatic, relativistic, and quantum electrodynamics interactions on the pair potential and thermophysical properties of helium *J. Chem. Phys.* **136** 224303

[14] May E F, Moldover M R, Berg R F and Hurly J J 2006 Transport properties of argon at zero density from viscosity-ratio measurements *Metrologia* **43** 247

[15] May E F, Berg R F and Moldover M R 2007 Reference viscosities of H_2, CH_4, Ar, and Xe at low densities *Int. J. Thermophys.* **28** 1085–110

[16] Berg R F and Moldover M R 2012 Recommended viscosities of 11 dilute gases at 25 C *J. Phys. Chem. Ref. Data* **41** 043104

[17] Berg R F, May E F and Moldover M R 2014 Viscosity ratio measurements with capillary viscometers *J. Chem. Eng. Data* **59** 116–24

[18] Pimentel-Rodas A, Galicia-Luna L A and Castro-Arellano J J 2016 Capillary viscometer and vibrating tube densimeter for simultaneous measurements up to 70 MPa and 423 K *J. Chem. Eng. Data* **61** 45–55

[19] Al-Siyabi I 2013 *Effect of Impurities on CO_2 Stream Properties* (Heriot-Watt University)

[20] Nazeri M, Chapoy A, Burgass R and Tohidi B 2018 Viscosity of CO_2-rich mixtures from 243 K to 423 K at pressures up to 155 MPa: new experimental viscosity data and modelling *J. Chem. Thermodyn.* **118** 100–14

[21] Liu Z, Trusler J P M and Bi Q 2015 Viscosities of liquid cyclohexane and decane at temperatures between (303 and 598) K and pressures up to 4 MPa measured in a dual-capillary viscometer *J. Chem. Eng. Data* **60** 2363–70

[22] Sanchez-Vicente Y, Emerson I, Glover R, Herbage O, Susial Martin R and Trusler J P M 2019 Viscosities of liquid hexadecane at temperatures between 323 K and 673 K and pressures up to 4 MPa measured using a dual-capillary viscometer *J. Chem. Eng. Data* **64** 706–12

[23] van den Berg H R, ten Seldam C A and van der Gulik P S 1993 Compressible laminar flow in a capillary *J. Fluid Mech.* **246** 1–20
[24] Kawata M *et al* 1991 Capillary viscometers, measurement of the transport properties of fluids pp 49–75
[25] Sutton C M and Clarkson M T 1994 A general approach to comparisons in the presence of drift *Metrologia* **30** 487
[26] Westman S F, Stang H G J, Løvseth S W, Austegard A, Snustad I, Størset S Ø and Ertesvåg I S 2016 Vapor-liquid equilibrium data for the carbon dioxide and nitrogen (CO_2 + N_2) system at the temperatures 223, 270, 298 and 303 K and pressures up to 18 MPa *Fluid Phase Equilib.* **409** 207–41
[27] Jiao F, Al Ghafri S Z S, Hughes T J and May E F 2020 Extended calibration of a vibrating tube densimeter and new reference density data for a methane-propane mixture at temperatures from (203 to 423) K and pressures to 35 MPa *J. Mol. Liq.* **310** 113219
[28] Larrain J and Bonilla C 1970 Theoretical analysis of pressure drop in the laminar flow of fluid in a coiled pipe *Trans. Soc. Rheol.* **14** 135–47
[29] Kestin J, Ro S and Wakeham W 1971 Reference values of the viscosity of twelve gases at 25° C *Trans. Faraday Soc.* **67** 2308–13
[30] Vogel E 2016 The viscosities of dilute Kr, Xe, and CO_2 revisited: new experimental reference data at temperatures from 295 K to 690 K *Int. J. Thermophys.* **37** 1–20
[31] Schäfer M 2016 *Improvements to Two Viscometers Based on a Magnetic Suspension Coupling and Measurements on Carbon Dioxide* (Ruhr-Universität Bochum, Diss)
[32] Vogel E and Barkow L 1986 Precision measurements of the viscosity coefficient of carbon dioxide between room temperature and 650 K *Z. Phys. Chem.* **267** 1038–43
Hendl S, Neumann A-K and Vogel E 1993 The viscosity of carbon dioxide and its initial density dependence *High Temp.-High Press.***25** 503–11
[33] Hellmann R 2014 *Ab initio* potential energy surface for the carbon dioxide molecule pair and thermophysical properties of dilute carbon dioxide gas *Chem. Phys. Lett.* **613** 133–8
[34] Laesecke A and Muzny C D 2017 Reference correlation for the viscosity of carbon dioxide *J. Phys. Chem. Ref. Data* **46** 013107